








Article

Torsion-Bar Antenna: A Ground-Based Detector for Low-Frequency Gravity Gradient Measurement

Satoru Takano ^{1,2,*}, Tomofumi Shimoda ^{1,†}, Yuka Oshima ¹, Ching Pin Ooi ¹, Perry William Fox Forsyth ¹, Mengdi Cao ³, Kentaro Komori ^{1,4}, Yuta Michimura ⁴, Ryosuke Sugimoto ¹, Nobuki Kame ⁵, Shingo Watada ⁵, Takaaki Yokozawa ⁶, Shinji Miyoki ⁶, Tatsuki Washimi ⁷ and Masaki Ando ^{1,4}

¹ Department of Physics, The University of Tokyo, Bunkyo-ku, Tokyo 133-0033, Japan; yuka.oshima@phys.s.u-tokyo.ac.jp (Y.O.); ooichingpin@gmail.com (C.P.O.)

² Department of Physics, Tokyo Institute of Technology, Meguro-Ku, Tokyo 152-8551, Japan

³ Department of Astronomy, Beijing Normal University, Beijing 100875, China

⁴ Research Center for the Early Universe (RESCEU), Graduate School of Science, The University of Tokyo, Bunkyo-ku, Tokyo 113-0033, Japan

⁵ Earthquake Research Institute, The University of Tokyo, Bunkyo-ku, Tokyo 113-0032, Japan

⁶ Institute for Cosmic Ray Research (ICRR), KAGRA Observatory, The University of Tokyo, Kashiwa 277-8582, Japan; yokozawa@icrr.u-tokyo.ac.jp (T.Y.)

⁷ Gravitational Wave Science Project (GWSP), Kamioka Branch, National Astronomical Observatory of Japan (NAOJ), Kamioka-cho, Hida City, Gifu 506-1205, Japan; tatsuki.washimi@nao.ac.jp

* Correspondence: takano@gw.phys.titech.ac.jp

† Current address: National Metrology Institute of Japan (NMIJ), National Institute of Advanced Industrial Science and Technology (AIST), Tsukuba, Ibaraki 305-8563, Japan.

Abstract: The Torsion-Bar Antenna (TOBA) is a torsion pendulum-based gravitational detector developed to observe gravitational waves in frequencies between 1 mHz and 10 Hz. The low resonant frequency of the torsion pendulum enables observation in this frequency band on the ground. The final target of TOBA is to observe gravitational waves with a 10 m detector and expand the observation band of gravitational waves. In this paper, an overview of TOBA, including the previous prototype experiments and the current ongoing development, is presented.

Keywords: gravitational wave; torsion pendulum; laser interferometer; cryogenics



Citation: Takano, S.; Shimoda, T.; Oshima, Y.; Ooi, C.P.; Forsyth, P.W.F.; Cao, M.; Komori, K.; Michimura, Y.; Sugimoto, R.; Kame, N.; et al. Torsion-Bar Antenna: A Ground-Based Detector for Low-Frequency Gravity Gradient Measurement. *Galaxies* **2024**, *12*, 78. <https://doi.org/10.3390/galaxies12060078>

Academic Editors: Eleonora Troja and Margo Aller

Received: 11 September 2024

Revised: 28 October 2024

Accepted: 18 November 2024

Published: 20 November 2024



Copyright: © 2024 by the authors. Licensee MDPI, Basel, Switzerland. This article is an open access article distributed under the terms and conditions of the Creative Commons Attribution (CC BY) license (<https://creativecommons.org/licenses/by/4.0/>).

1. Introduction

Since the first detection of gravitational waves (GWs) by Advanced LIGO [1], gravitational wave astronomy has continued to develop and multi-messenger astronomy has gained attention. The sources of the detected GWs by the ground-based detectors are the coalescence of binary systems with source masses in the range of $1 M_{\odot}$ – $100 M_{\odot}$, which correspond to the observed frequency band of 10 Hz–1 kHz [2]. Another observation band of interest is in the range of 1 mHz–10 Hz. In this frequency band, some target sources are expected, such as the merger of Intermediate Mass Black Holes (IMBHs) with masses in the order of $10^2 M_{\odot}$ – $10^5 M_{\odot}$, or the Stochastic Gravitational Wave Background (SGWB) from the early universe. To observe GWs in this frequency band, space interferometric detectors such as LISA [3] and DECIGO [4] have been proposed.

Several ground-based detectors for observing GWs in frequencies between 1 mHz and 10 Hz have been proposed, such as atomic interferometers [5,6] and super-conductive gravity gradiometers [7,8]. One such detector is the Torsion-Bar Antenna (TOBA), which uses torsion pendulums to observe GWs [9]. Thanks to the low resonant frequency of the torsion pendulums, TOBA is sensitive to the gravitational waves in the frequency band of 1 mHz–10 Hz. The main goal of TOBA is to achieve the sensitivity of $10^{-19} / \sqrt{\text{Hz}}$ at 0.1 Hz. This sensitivity allows us to detect IMBH binary mergers at cosmological distances. Thanks

to the ground-based configuration, TOBA has the advantage of better accessibility and lower cost than the space detectors in the similar frequency band.

In this paper, we provide an overview of TOBA. The principle of operation and scientific targets of the TOBA are in Section 2. Next, the results of the previous prototypes and the related developments are explained in Section 3. In Section 4, we introduce the upcoming prototype, Phase-III TOBA, and present recent developments.

2. Overview of TOBA

2.1. Principle of TOBA

The theory guiding the usage of torsion pendulums to detect GWs predates the TOBA detector by several decades [10,11]. A detailed derivation of the principal of detection is provided in Appendix A but summarized here.

Figure 1 shows a basic configuration of TOBA, with bars suspended in the horizontal xy -plane. Here, we focus on the rotational motion of a bar around the z -axis, θ .

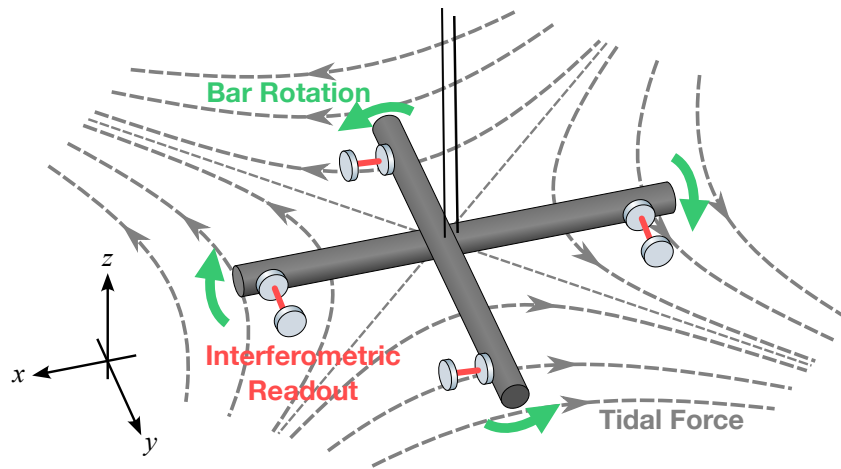


Figure 1. Principle of TOBA. Two test mass bars are suspended in the horizontal plane independently and orthogonally. Dashed lines indicate the gravitational tidal forces induced by a GW coming along the z -axis, and green arrows show the rotation directions of the bars. The rotation angles of the bars are measured by interferometers.

Suppose that a GW comes along the z -axis,

$$h_{ij}^A = h_A e_{ij}^A \cos 2\pi ft, \quad (1)$$

where

$$e_{ij}^+ = \begin{pmatrix} 1 & 0 & 0 \\ 0 & -1 & 0 \\ 0 & 0 & 0 \end{pmatrix}, \quad e_{ij}^\times = \begin{pmatrix} 0 & 1 & 0 \\ 1 & 0 & 0 \\ 0 & 0 & 0 \end{pmatrix} \quad (2)$$

are the polarization tensors of GW. Considering the forces acting on each discrete element of the bar, the frequency response function is given by

$$H_+(f) := \frac{\theta}{h_+} = 0, \quad H_\times(f) := \frac{\theta}{h_\times} \simeq \frac{1}{2} \frac{f^2}{f_0^2(1 + i\phi_{\text{rot}}) - f^2}, \quad (3)$$

where f_0 is the resonant frequency of the torsion pendulum and ϕ_{rot} is the loss angle of the suspension wire.

The differential response of each bar is generated by the perpendicular orientation of each bar. By matching mechanical parameters between the two pendulums, such as overlapping the center of mass and maintaining a similar mechanical response, noises can be rejected from the GW measurement provided by the differential motion of the bars. This rejection of common noises between the two pendulums is referred to as common mode

rejection of the detector, and stands as one of the significant advantages of using a twin torsional pendulum detector setup for GW detection, such as the TOBA.

2.2. Target Sensitivity of TOBA

The final target sensitivity of TOBA is $10^{-19} / \sqrt{\text{Hz}}$ at 0.1 Hz in strain, which is determined for observing the targets mentioned in the following sections. To achieve this sensitivity, a 10 m torsion-bar detector, The Final TOBA, is proposed. The designed noise budget is shown in Figure 2.

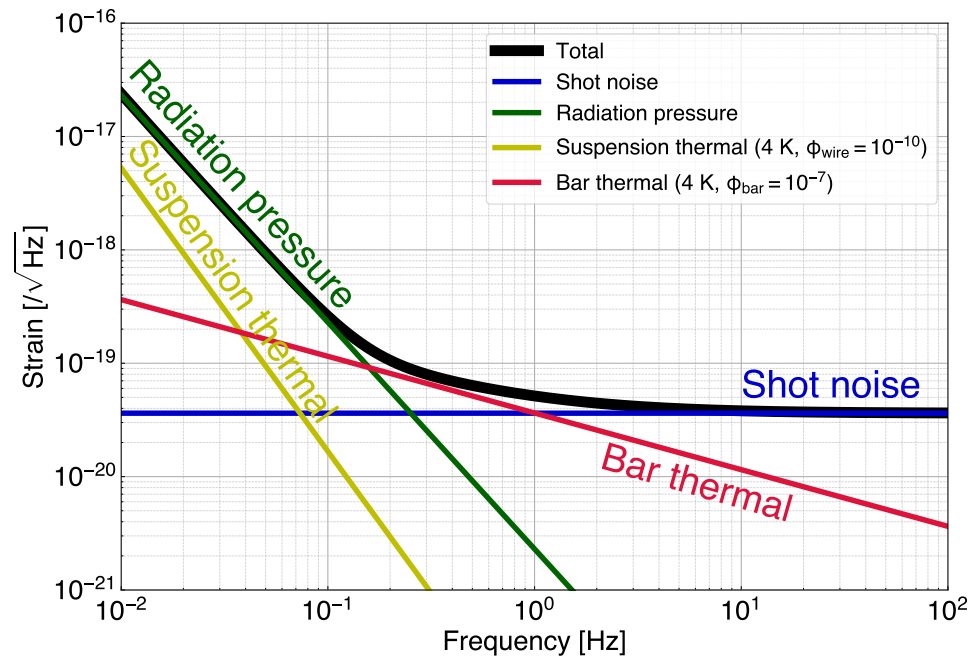


Figure 2. The design sensitivity of the Final TOBA [9]. The blue and green lines show the photon shot noise and radiation pressure noise, respectively. The yellow and red lines indicate the thermal noise of the suspension wire and the test mass bars. The black line is the sum of all noises.

The Final TOBA consists of two large torsion pendulums, as shown in Figure 1. Each bar is made of aluminum with a length of 10 m and a diameter of 0.6 m, which correspond to a mass of 7.6×10^3 kg and moment of inertia of 6.4×10^4 kg m². The resonant frequency of the rotational mode is designed to be 1 mHz and the loss of the suspension wire and the loss of the internal modes of the bar are required to be 10^{-10} and 10^{-7} , respectively. Each bar and its suspension wire are to be kept at a cryogenic temperature of 4 K to reduce thermal noise. The rotation of the bars is to be measured by a pair of Fabry–Pérot cavities at both ends of the bars. Each cavity has a finesse of 100 and the input laser power to the cavities is to be set as 10 W. Two pendulums are to have as a close mechanical response as possible, which can eliminate or reduce noises familiar to both pendulums.

Considering all these noises, the sensitivity of the Final TOBA is predicted to be limited by the quantum noise (shot noise and radiation pressure noise) and thermal noise of the bar [9].

2.3. Target Sources of Gravitational Waves for TOBA

One of the main target sources of GWs in the frequency band of 1 mHz–10 Hz is the coalescence of IMBH binary systems. Their existence has only been reported through indirect mass estimation, and direct observation of GWs from these systems is of great importance for the study of IMBHs. For example, observation of GWs from IMBHs would provide us with some hints about the origin and formation of supermassive black holes at the center of galaxies [12,13]. With the Final TOBA’s target sensitivity, the observation range

of IMBH binary mergers with their source mass $10^5 M_{\odot}$ reaches 10 Gpc, which corresponds to the redshift of $z \sim 2.4$ [9].

Another important target of GWs in this frequency band is the SGWB from the early universe. Unlike electromagnetic waves, GWs can pass through the radiation field before recombination and see the universe before 0.38 Myr from the Big Bang. In terms of the dimensionless energy density of GWs, Ω_{GW} , the sensitivity of $10^{-19} / \sqrt{\text{Hz}}$ corresponds to $\Omega_{\text{GW}} \simeq 10^{-7}$ with a one-year observation period [9], which is a better constraint than the upper bound set by Big Bang Nucleosynthesis (BBN) [14].

2.4. Geophysical Target of TOBA

Since GW detectors respond to the gravity gradient, the measured signal can also originate from terrestrial sources such as the ground and the atmosphere. In terms of GW detection, such a signal is called Newtonian Noise (NN) because the gravity gradient induced by the terrestrial sources cannot be distinguished from the effect of GWs [15]. It has also been proposed that with a moderate sensitivity of $10^{-15} / \sqrt{\text{Hz}}$, the measured terrestrial gravity gradient has great geophysical importance [16]. Here, we introduce two related cases.

2.4.1. Newtonian Noise Measurement

NN is a fundamental noise source for GW detectors. For future ground-based GW detectors, NN is assumed to be the dominant noise source in frequency bands below 10 Hz [17,18], and its mitigation method is discussed in [19,20]. Several models describe the mechanism of NN generation [21–24]. However, so far, NN has not been measured directly. Therefore, direct measurement of NN and test of the models are essential for GW detectors on the ground.

Some models predict that around 0.1 Hz, the amplitude level of NN grows up to the order of $10^{-15} / \sqrt{\text{Hz}}$ [22,25]. Therefore, TOBA is expected to detect NN in this frequency band and partially justify the model and cancellation scheme.

2.4.2. Early Earthquake Detection

It is proposed that transient changes in gravitational fields introduced by large earthquakes can be detected by gravimeters and gravity gradiometers [26]. This scheme pays attention to the change that occurs on the timescale of $\sim 10\text{s}–100\text{s}$, which corresponds to the frequency band of TOBA. Because the change in the gravitational field propagates with the speed of light, the detection of earthquakes with TOBA is expected to be faster than the current warning scheme, which uses seismic P-waves with a velocity of $\sim 1\text{ km/s}–10\text{ km/s}$.

It has also been pointed out that TOBA has an advantage in detecting earthquakes. Gravimetric measurements, such as using gravimeters, seismometers, and tiltmeters, are considered to be ineffective for early earthquake detection due to decreased sensitivity caused by instrument acceleration [27,28]. On the other hand, TOBA is expected to avoid this cancellation because instrument acceleration does not affect gravity gradient measurements.

In previous research, the possibility of detecting earthquakes with TOBA was studied [16,29]. It is expected that with a moderate sensitivity of $\sim 10^{-15} / \sqrt{\text{Hz}}$ at 0.1 Hz, the detectability is almost the same as the current system.

3. Prototype Developments

To reach the target sensitivity of the Final TOBA, studies of each component and demonstrations of noise reduction have been performed with small prototypes. The achieved sensitivity of these prototypes are summarized in Figure 3.

In this section, we briefly introduce these prototype developments and their achievements.

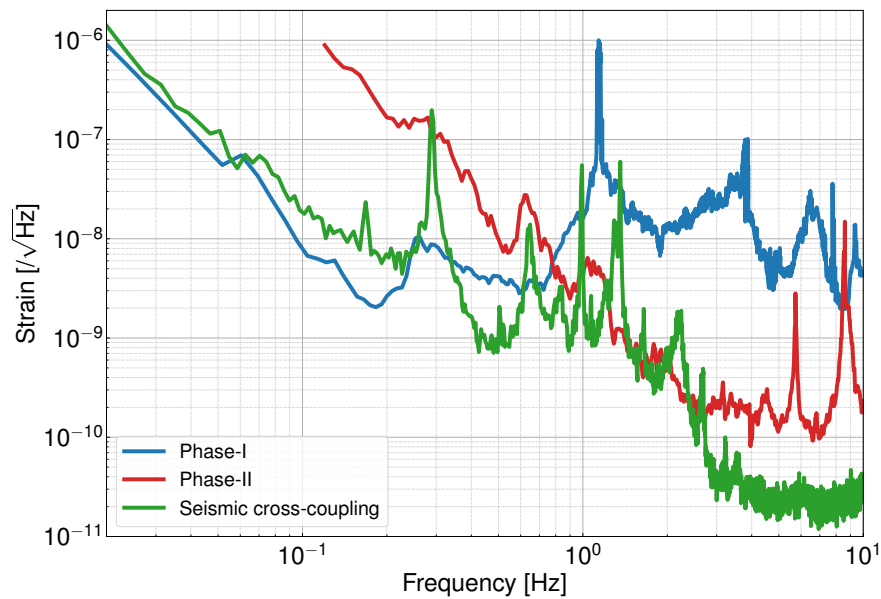


Figure 3. The sensitivity of prototype experiments. The blue and red curves are the achieved sensitivities of Phase-I [30] and Phase-II [31]. The green curve shows the sensitivity obtained in the experiment of seismic cross-coupling reduction [32].

3.1. Phase-I TOBA

The first prototype, named Phase-I TOBA, was developed in 2010 [33] as a proof of concept. The test mass bar, with a length of 22.5 cm, was suspended by superconducting magnet levitation. Though there is no restoring force in the rotational degree of freedom in principle, the actual resonant frequency was ~ 5 mHz due to the gradient of the magnetic field induced by the levitating magnet. The rotational motion was measured by a Michelson interferometer on the ground. The configuration of the bar and the interferometer is shown in Figure 4.

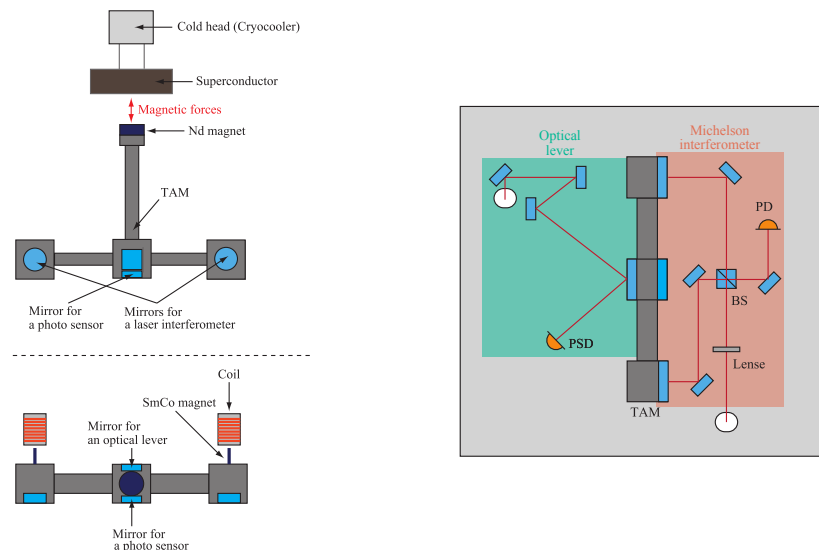


Figure 4. The configuration of Phase-I TOBA. (Left) Test mass bar of Phase-I TOBA. A single test mass bar was suspended by superconducting magnet levitation. The test mass was 22.5 cm bar made of aluminum. Many mirrors were attached to monitor the motion. (Right) The optical configuration of Phase-I TOBA. The best sensitivity was obtained with a Michelson interferometer consisting of the end mirrors attached to both ends of the bar and the other optics on an optical bench fixed on the vacuum chamber. These figures were adapted from [33] and modified for this paper.

The sensitivity of the Phase-I prototype was limited by ambient magnetic field fluctuations and seismic cross-coupling. Below 0.1 Hz, the magnet for levitating the test mass bar coupled with the ambient magnetic field and induced a torque noise to the test mass bar. Above 0.1 Hz, the translational seismic motion was transferred to the rotational signal of the test mass bar due to the relative tilt of the mirrors attached on the test mass for interferometric readout. The achieved sensitivity was $\sim 10^{-8} / \sqrt{\text{Hz}}$ at 0.1 Hz.

With this sensitivity, a search for SGWB was performed, and the upper limit was set to $\Omega_{\text{GW}} h_0^2 < 1.9 \times 10^{17}$ at 0.035 Hz–0.830 Hz [30,33].

3.2. Phase-II TOBA

The second prototype, Phase-II TOBA, was developed in 2015 [31,34]. In this prototype, two test mass bars with a length of 24 cm were used, and they were suspended by metal wires in order to reduce magnetic noise coupling, which was one of the dominant noise sources in Phase-I TOBA. Two test mass bars were suspended orthogonally with double wires from an intermediate mass and consisted of double-stage pendulums. At the suspension point, an active feedback system was introduced for reducing seismic vibration. It consisted of six seismometers and hexapod actuators.

The rotational motion was measured by fiber Michelson interferometers constructed on an optical bench, which was also suspended from the intermediate mass. With these fiber interferometers, not only the horizontal rotation but also the vertical rotational motions were measured. Thanks to this configuration called a multi-output configuration, the detection volume and angular accuracy can be improved because the signal from each degree of freedom compensates for the blind spots of the other degrees of freedom. The configuration of the test masses and interferometric sensors are shown in Figure 5.

The sensitivity of Phase-II TOBA was limited by seismic coupling noise and the phase noise induced by the vibration of the optical fiber within the readout interferometer. The achieved sensitivity was $\sim 10^{-10} / \sqrt{\text{Hz}}$ at 3 Hz–8 Hz.

With this sensitivity, the upper limit on SGWB was set to $\Omega_{\text{GW}} h_0^2 < 1.2 \times 10^{20}$ at 2.6 Hz [34]. Also, the existence of 200 M_{\odot} IMBH binaries was excluded within $r < 2.1 \times 10^{-4}$ pc [31].

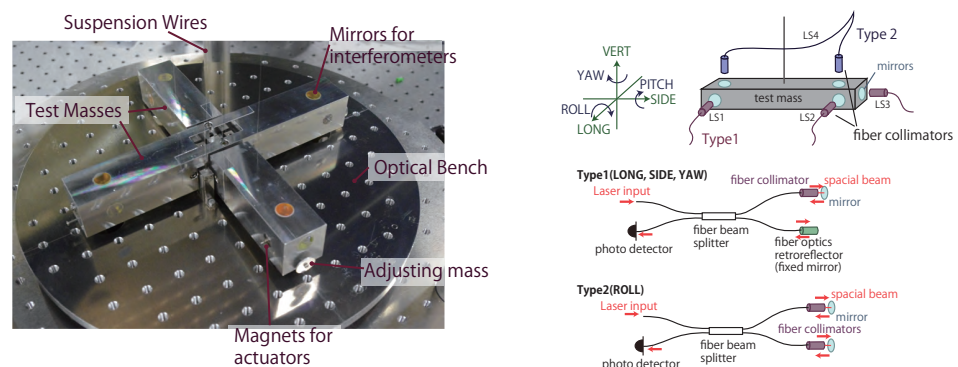


Figure 5. The configuration of Phase-II TOBA. (Left) Test mass bars of Phase-II TOBA. Two test mass bars were suspended by two suspension wires. Each test mass was 24 cm long and made of aluminum. Many mirrors were attached for fiber interferometer. (Right) The optical configuration of Phase-II TOBA. Fiber Michelson interferometers were utilized to measure multiple rotation degrees of freedom of the test mass bars. These figures were adapted from [31].

3.3. Research on Seismic Cross-Coupling Reduction

For understanding the translational seismic noise coupling and reducing it, an experiment with a double-stage pendulum was performed in 2017 [32]. This experiment consisted of a test mass bar and free-space Michelson interferometer on an optical bench to measure the horizontal rotation of the bar. The bar was a 20 cm long fused silica block with an optical coating on a well-polished surface. By making the interferometer with this flat

surface, the relative tilt between the mirror surface at both ends of the bar was reduced, which was the main source of the cross-coupling in Phase-I TOBA. The configuration of the test mass and the interferometer is shown in Figure 6.

This experiment examined the model of the cross-coupling of the seismic noise, and demonstrated the reduction scheme of the coupling by tuning the tilt angle of the test mass bar and the optical bench. The achieved cross-coupling function was 5×10^{-6} rad/m at 0.1 Hz. Even though these values are not sufficient for the Final TOBA, this work established the basic strategy for reducing the coupling transfer function.

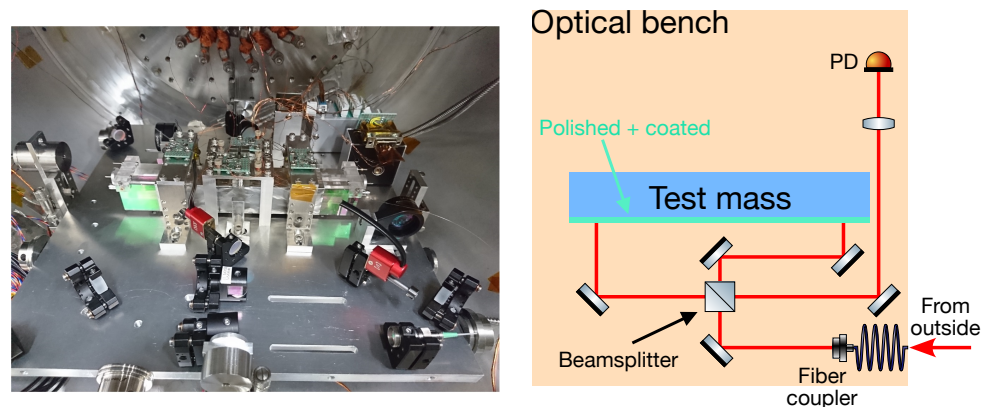


Figure 6. The setup for research on seismic cross-coupling reduction. **(Left)** A picture of the test mass bar and the optics. The test mass bar was made of fused silica, and its front surface was polished and HR-coated. The length of the test mass was 20 cm, and it was suspended by a single wire. **(Right)** The optical configuration of this setup. A Michelson interferometer consisted of the optics on the suspended optical bench and the surface of the test mass.

4. Next Prototype: Phase-III TOBA

Following these prototype experiments, an upgraded prototype, Phase-III TOBA, is currently under development. We consider Phase-III TOBA to be just one step before the Final TOBA, and the configuration is closer to it than the previous experiments. The target of Phase-III TOBA is to reach a sensitivity of about $10^{-15} / \sqrt{\text{Hz}}$ at 0.1 Hz with small-scale (~ 30 cm) test mass bars. In addition to the noise reduction mentioned above, the reduction in the thermal noise by introducing a cryogenic system is one of the important issues to be solved here. Furthermore, with the target sensitivity, we expect to achieve scientific results, such as the detection of earthquakes and direct measurement of NN.

4.1. Design Overview

The configuration of Phase-III TOBA is shown in Figure 7. It consists of the following three parts:

- A cryogenic suspension system;
- An active vibration isolation system;
- An interferometric readout system.

Here, we describe each system.

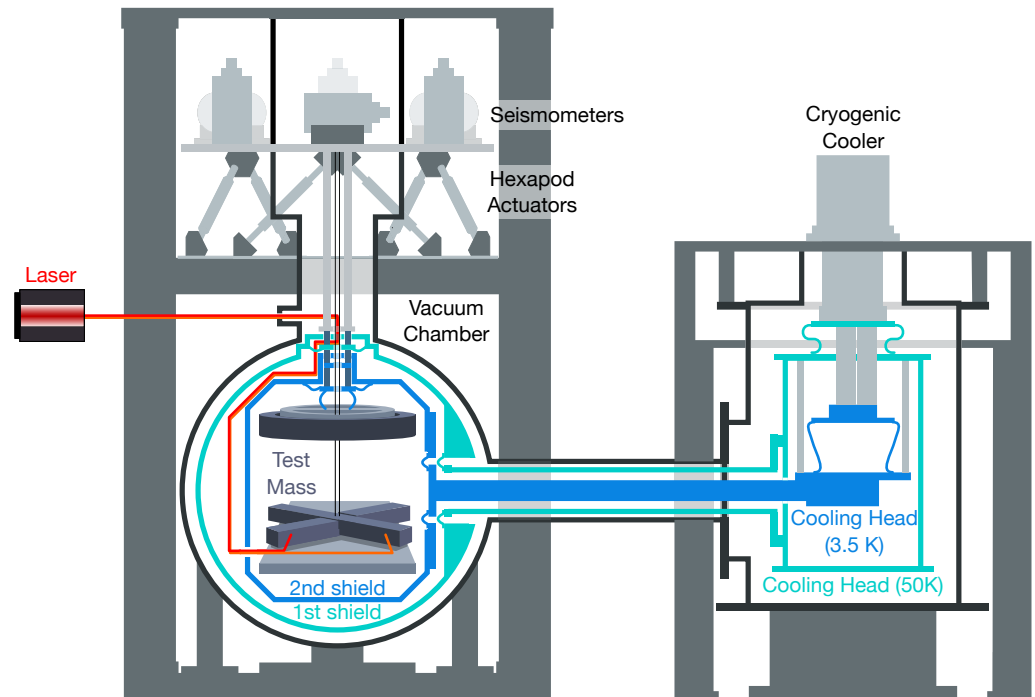


Figure 7. Configuration of Phase-III TOBA. Inside a vacuum chamber, two radiation shields are connected to the cryocooler surrounding the suspension system. Two test mass bars are suspended by a wire with a high Q value. At the suspension point, an active vibration isolation system is implemented. The rotation of the bars are measured by an interferometer.

4.1.1. Cryogenic Suspension System

The cryogenic system is one of the essential parts of Phase-III TOBA for reducing thermal noise. The required temperature for Phase-III TOBA is set to 4 K, and it is also desirable to finish the cooling within an acceptable time for operation. Another important point is to suppress additional noises introduced by the cooling system, such as vibrations from the cooler.

The cooling system consists of a cryocooler, two radiation shields, and a main suspension system, as shown in Figure 7. A pulse tube cooler is used to cool the radiation shields to 50 K (first shield) and 3.5 K (second shield), respectively, and the intermediate masses are connected to the second shield via high-purity aluminum (6 N) wires (heatlinks). The test mass bars are cooled by thermal radiation (>100 K) and heat conduction through the suspension wires (<100 K). The suspension wires of the test mass bars are made of silicon, which is known to have low mechanical loss ($\phi < 10^{-8}$) at cryogenic temperatures [35].

Because each test mass is to be suspended by a single silicon fiber, the thermal exchange is not efficient and the cooling time down to 4 K is approximately 14 days [29]. On the other hand, the suspension fibers insulate the test mass bars well from the surroundings and reduce other temperature fluctuations of the bars.

4.1.2. Active Vibration Isolation System

To suppress the seismic vibration, an active vibration isolation system (AVIS) is implemented at the suspension point.

AVIS is a feedback system that consists of multiple sensors and hexapod actuators. Six seismometers are arranged to monitor all degrees of freedom of the suspension table. The signals from the seismometers are processed by a digital system, and fed back to hexapod actuators, which consist of six piezoelectric actuators attached below the table. The actuators are configured to actuate the table in all degrees of freedom, including translation along three axes and rotation around three axes.

AVIS is also utilized for suppressing the vibration of the cooler introduced via the heatlinks attached to IMs. Heatlinks on IMs are not directly connected to the second shield,

but first attached to a bypass stage, which is connected to the suspension table via thermal insulation rods, and then connected to the second shield. By connecting the heatlinks on the stage, the feedback system reduces not only the seismic vibration, but also vibrations transferred via the heatlinks.

The target performance of AVIS is to reduce the vibration level to below $10^{-7} \text{ m}/\sqrt{\text{Hz}}$ at 0.1 Hz for reducing the seismic cross-coupling noise [32], and to below $10^{-10} \text{ m}/\sqrt{\text{Hz}}$ at 1 Hz to suppress nonlinear vibration noise [36].

4.1.3. Interferometric Readout System

To achieve the target sensitivity, we use Fabry–Pérot cavities to measure the motion of the bars. The surface of the test mass bar is polished and coated so that it works as mirrors, to reduce the relative tilt of the mirrors which introduces the cross-coupling. The other mirrors, which form Fabry–Pérot cavities with the surface of the bars, are implemented on an optical bench.

One issue concerning the readout system is the noise of the readout optics. As the phase noise of the readout interferometer limited the sensitivity of Phase-II TOBA, the readout noise of the interferometer, induced by ambient noise, such as the vibration coupling and the temperature drift, should be reduced sufficiently. The required sensitivity for the readout noise of the interferometer is set to $6 \times 10^{-17} \text{ m}/\sqrt{\text{Hz}}$ at 0.1 Hz. To achieve this requirement, a cryogenic-compatible monolithic interferometer is planned to be introduced.

4.2. Target of Phase-III TOBA

With the systems mentioned above, the design sensitivity of Phase-III TOBA is shown in Figure 8.

As we mentioned in Section 2, Phase-III TOBA has the potential to detect earthquakes and measure NN directly with a sensitivity of $10^{-15}/\sqrt{\text{Hz}}$.

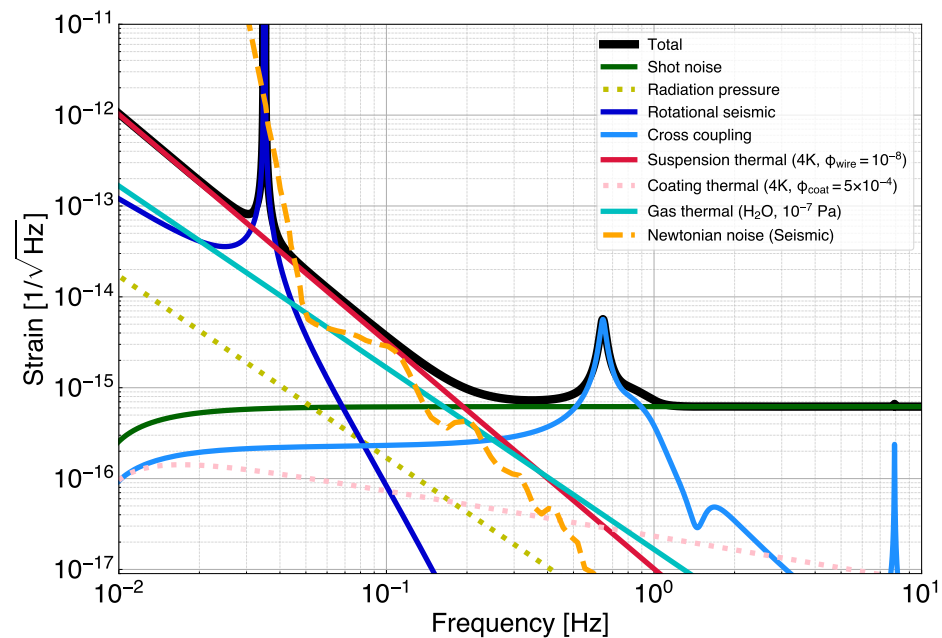


Figure 8. The designed noise budget of Phase-III TOBA. The green line shows photon shot noise. The red line is the thermal noise of the suspension wire. The dark blue line and the sky blue line are the seismic noise from the ground rotation and the ground translation, respectively. The cyan line indicates the thermal noise from the residual water molecules. The black line is the sum of these noises. The orange dashed line indicates the estimated NN level of KAGRA site [22] to be measured with Phase-III TOBA.

4.2.1. Newtonian Noise Measurement

The estimated level of NN is in the order of $10^{-15}/\sqrt{\text{Hz}}$ around 0.1 Hz. Therefore, it is expected that Phase-III TOBA can measure NN directly with the target sensitivity. Although the frequency band in which Phase-III TOBA can observe NN is below the observation band of the ground-based interferometric detectors, measurement with Phase-III TOBA is useful for testing the models of NN and demonstrating its mitigation scheme.

4.2.2. Gravity Gradient Fluctuation Induced by Earthquakes

Previous research investigated the detectability of earthquakes with Phase-III TOBA's target sensitivity [16,29]. It has been shown that for earthquakes with a magnitude of M_w 7, we can detect them ~ 10 s faster than the current warning system if they happen ~ 100 km away. To identify the location of the center of the earthquake with the same precision as with the current system, two detectors separated by ~ 75 km are necessary.

4.3. Current Achievements

We have been developing Phase-III TOBA for years and have achieved some of the goals described in Section 4.1. We briefly introduce the current achievements of these systems.

4.3.1. Cryogenic Suspension System

The basic cryogenic suspension system was demonstrated in 2020 [29]. The measured cooling curve is shown in Figure 9. The test mass bars were successfully cooled down to 6.1 K in 10 days. Because the silicon suspension wire is still under development, in this demonstration, CuBe wires were used for the suspension of the bars, and 6N aluminum heatlinks were attached between the intermediate mass and the test masses to increase the heat conductance.

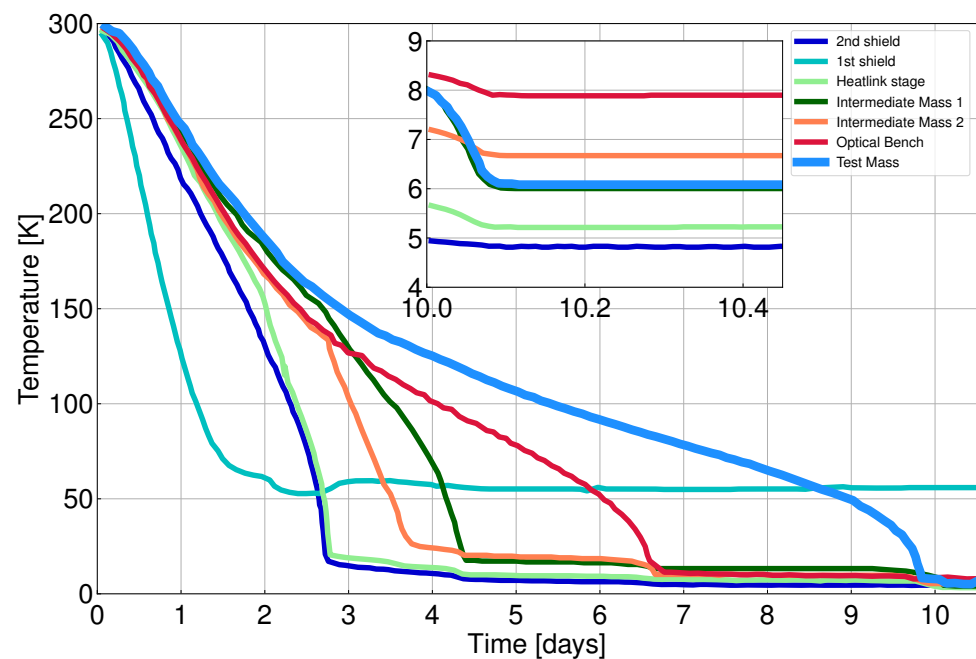


Figure 9. The cooling curve of the cryogenic torsion pendulum measured in [29]. The sky blue curve shows the temperature of the test mass bar. The test mass was cooled down to 6.1 K in 10 days.

4.3.2. Active Vibration Isolation System

A prototype of the vibration isolation system was developed and the performance was tested in 2019 without the suspension system. The achieved performance is shown in Figure 10. The vertical seismic vibration was suppressed by 10^3 around 0.7 Hz and the

horizontal vibration by 3×10^{-2} around 1.7 Hz. The performance was still not sufficient to meet the requirement. One reason was tilt-horizontal coupling [37] in frequencies below 0.5 Hz, which smeared the true signal of the horizontal motion and introduced instability in the control. Another reason was the parasitic resonance modes of the supporting frame of the system, which prevented us from increasing the feedback gain and resulted in an insufficient suppression ratio.

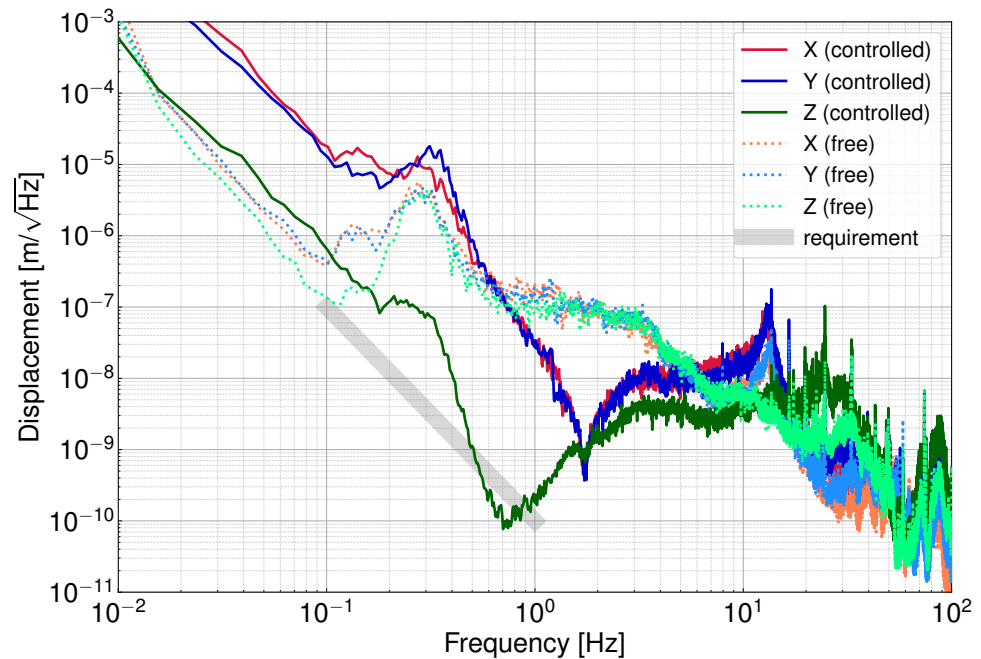


Figure 10. The achieved performance of AVIS. The gray line indicates the requirement for AVIS. The red, blue, and green dashed lines are the vibration spectra without control in the x -, y -, and z -axes, respectively. The red, blue, and green solid lines show the vibration spectra with control of AVIS in the x -, y -, and z -axes, respectively.

4.3.3. Interferometric Readout System

The cryogenic monolithic interferometer was demonstrated in 2024 [38]. In this demonstration, the readout optics made of silicon were glued on a silicon breadboard and consisted of a monolithic interferometer with one test mass bar fixed on the breadboard as well. The interferometer was operated stably at 12 K and achieved the sensitivity of $3.6 \times 10^{-14} \text{ m}/\sqrt{\text{Hz}}$ at 0.1 Hz. The performance was limited by the seismic noise on the horizontal axis. The sensitivity and the estimated noise contributions are shown in Figure 11.

Another method to measure the rotation of the bar, the Cavity-Amplified Angular Sensor (CAAS), was also proposed [39]. CAAS utilizes an optical cavity for the amplification of the angular signal, and has better sensitivity than normal angular measurement methods, such as optical levers. Compared to the rotation measurements by differential Fabry–Pérot cavities, direct rotation measurement by CAAS has the advantage of smaller cross-coupling noise. So far, the basic principle has been demonstrated [39] and further improvements are ongoing.

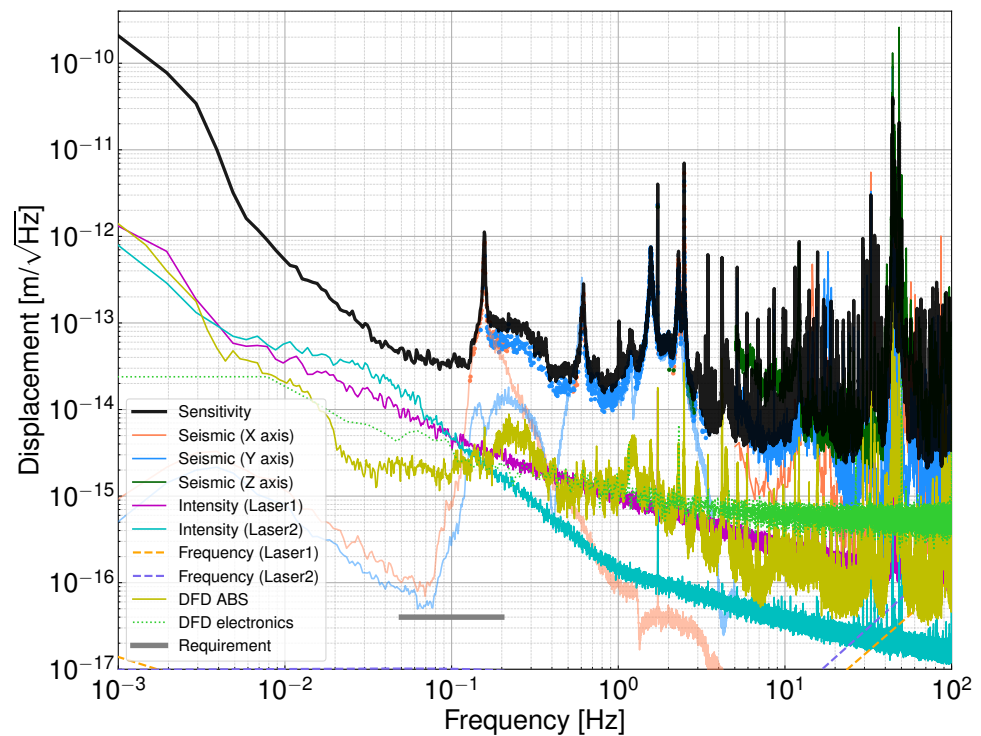


Figure 11. The achieved sensitivity of the cryogenic monolithic interferometer [38]. The sensitivity shown as the black curve is limited by seismic noise (red in the x -axis, blue in the y -axis, and green in the z -axis). The gray line indicates the requirement for the monolithic interferometer.

4.4. Beyond Phase-III TOBA

As we see in the previous section, some of the techniques necessary for Phase-III TOBA have been demonstrated. Although they still need further improvement, the outlook toward the Final TOBA should be discussed in parallel.

To scale the detector up to 10 m in length, there will be many difficulties. For example, suspending such gigantic objects with a single fiber requires special attention to the mechanical design, such as tuning resonant frequency while maintaining low mechanical loss and sufficient tensile strength. Cooling such a enormous system is another potential issue. Solving such technical issues will require additional study and substantial costs, which could diminish its advantage over space detectors.

Nevertheless, TOBA has its own valuable scientific targets, such as NN measurement and earthquake detection, which cannot be observed with space detectors. These targets are expected to be measured with Phase-III TOBA if all the technical achievements are realized, and future TOBA setups will obtain more precise results.

5. Conclusions

In this paper, an overview of TOBA is presented. The final target of TOBA is described, and the current status of the technical demonstration is provided.

A small prototype named Phase-III TOBA is under development to achieve the sensitivity of $10^{-15} / \sqrt{\text{Hz}}$. With this sensitivity, geophysical targets such as earthquakes and NN are expected to be detectable. To achieve the target sensitivity, technical demonstrations of each subsystem are ongoing.

After achieving the target of Phase-III TOBA, we will move on to building a large-scale detector to achieve the sensitivity of $10^{-19} / \sqrt{\text{Hz}}$. This detector would enable us to observe GWs from the merger of IMBH binaries.

Author Contributions: Conceptualization, S.T., T.S. and M.A.; methodology, S.T., T.S., Y.O., C.P.O. and M.C.; software, S.T. and T.S.; validation, K.K., Y.M. and M.A.; formal analysis, S.T. and T.S.; investigation, S.T., T.S. and M.A.; resources, S.T. and T.S.; data curation, M.A.; writing—original draft preparation, S.T.; writing—review and editing, S.T., C.P.O., P.W.F.F., Y.O., K.K., N.K., T.S. and M.A.; visualization, S.T.; supervision, M.A.; project administration, M.A.; funding acquisition, all authors. All authors have read and agreed to the published version of the manuscript.

Funding: JSPS KAKENHI, Grants Number JP16H03972, JP24244031, JP18684005, and JP22H01246. This work was also supported by the MEXT Quantum Leap Flagship Program (MEXT Q-LEAP), Grant Number JPMXS0118070351.

Data Availability Statement: Dataset available on request from the authors.

Acknowledgments: We would like to thank Takafumi Ushiba (ICRR) for helpful discussion about cryogenics. We also would like to thank Yoichi Aso (NAOJ) for offering materials for the cryogenic experiments. Finally, we would like to acknowledge the great support of Shigemi Otsuka and Togo Shimozawa (The University of Tokyo) for making the mechanical parts in the experiments.

Conflicts of Interest: The authors declare no conflicts of interest.

Appendix A. Derivation of the Response of a Torsion Pendulum to Gravitational Waves

In this section, we derive the mechanical response of a torsion pendulum to gravitational waves.

Appendix A.1. Torque Induced by Gravitational Waves

Consider a GW coming along the z-axis described by Equations (1) and (2). Within a region whose scale is small enough compared to the wavelength of the GW, the force dF_{GW}^i induced by the GW acting on a particle with mass m at x^i is given by [40]

$$dF_{\text{GW}}^i = \frac{1}{2} m \ddot{h}_j^i x^j. \quad (\text{A1})$$

Here, $h_{\mu\nu}$ ($\mu, \nu \in \{0, 1, 2, 3\}$) are the small deviations of the metric tensor $g_{\mu\nu}$ from flat space-time $\eta_{\mu\nu} = \text{diag}(-1, +1, +1, +1)$, and h_{ij} ($i, j \in 1, 2, 3$) are the spatial components of $h_{\mu\nu}$. Up to linear order of $h_{\mu\nu}$, the indices of $h_{\mu\nu}$ are raised by $\eta^{\mu\nu}$. In particular, h_j^i are given by

$$h_j^i = \eta^{i\alpha} h_{\alpha j} = \delta^{ik} h_{kj} = h_{ij}. \quad (\text{A2})$$

Next, consider a bar located along the x-axis, as shown in Figure 1. Using Equation (A1), the force induced by the GW acting on a discrete element of the bar dV at ζ^i is given by

$$dF_{\text{GW}}^i = \frac{1}{2} \rho dV \ddot{h}_j^i \zeta^j, \quad (\text{A3})$$

where ρ is the density of the bar and ζ^i is the location of dV , whose origin is on the center of mass of the bar. The energy stored in dV by dF_{GW} is given by integrating dF_{GW} along ζ^i ,

$$dU_{\text{GW}} = - \int_0^{\zeta^i} d\zeta'_i dF_{\text{GW}}^i = \int_0^{\zeta^i} d\zeta'_i \frac{1}{2} \rho dV \ddot{h}_j^i \zeta^j = \frac{1}{4} \rho dV \ddot{h}_{ij} \zeta^i \zeta^j. \quad (\text{A4})$$

Then, integrating dU_{GW} over all the volume of the bar, we obtain the total energy stored in the bar U_{GW} by

$$U_{\text{GW}} = \int_V dU_{\text{GW}} = \frac{1}{4} \ddot{h}_{ij} \int_V dV \rho \zeta^i \zeta^j. \quad (\text{A5})$$

A torque on the bar is the rate of change of the energy related to the rotation θ . That is,

$$N_{\text{GW}} = - \frac{\partial U_{\text{GW}}}{\partial \theta} = \frac{1}{4} \ddot{h}_{ij} q^{ij}. \quad (\text{A6})$$

Here, q^{ij} is the quadrupole moment of the bar defined as

$$q^{ij} = \int_V dV \rho \left(\zeta^i w^j + \zeta^j w^i - \frac{2}{3} \delta^{ij} \zeta^k w_k \right), \quad (\text{A7})$$

where w^i is the mode function and in the case of the rotation around z-axis,

$$w^i = \begin{pmatrix} -y \\ x \\ 0 \end{pmatrix}. \quad (\text{A8})$$

Substituting Equation (A8) into Equation (A7), we obtain the components of the quadrupole moment as follows:

$$q_+ := q_{11} = -q_{22} = - \int_V dV \rho 2xy, \quad (\text{A9})$$

$$q_\times := q_{12} = q_{21} = \int_V dV \rho (x^2 - y^2). \quad (\text{A10})$$

Using Equations (A6), (A9), and (A10), the torque on the bar induced by GWs is written as

$$N_{\text{GW}} = \frac{\ddot{h}_{11} - \ddot{h}_{22}}{4} q_+ + \frac{1}{2} \ddot{h}_{12} q_\times. \quad (\text{A11})$$

Substituting Equations (1) and (2) into Equation (A11), we obtain

$$N_{\text{GW}} = \frac{\ddot{h}_+}{2} q_+ + \frac{\ddot{h}_\times}{2} q_\times. \quad (\text{A12})$$

Appendix A.2. Mechanical Response of a Torsion Pendulum

We consider the frequency response of the torsion pendulum. The equation of motion about θ is given by

$$I\ddot{\theta}(t) + \kappa\theta(t) = N_{\text{GW}}(t). \quad (\text{A13})$$

Here, I is the moment of inertia of the bar around the rotational axis (z-axis), and κ is the spring constant of the suspension wire in the torsional mode. Applying Fourier transformation to Equation (A13), we obtain

$$\frac{\theta(f)}{N_{\text{GW}}(f)} = \frac{1}{\kappa(1 + i\phi_{\text{rot}}) + (2\pi f)^2 I} = \frac{1}{4\pi^2 I (f_0^2(1 + \phi_{\text{rot}}) + f^2)}, \quad (\text{A14})$$

where

$$f_0 := \frac{1}{2\pi} \sqrt{\frac{\kappa}{I}} \quad (\text{A15})$$

is the resonant frequency of the rotation mode. Here, the loss angle ϕ_{rot} is the imaginary part of the spring constant κ , which is introduced to describe mechanical energy loss of the suspension wire. Plugging Equation (A12) into Equation (A14), we obtain

$$\theta(f) = \left(\frac{q_+}{2I} h_+(f) + \frac{q_\times}{2I} h_\times(f) \right) \frac{f^2}{f_0^2(1 + i\phi_{\text{rot}}) - f^2} \quad (\text{A16})$$

$$= \sum_A H_A(f) h_A(f) \quad (\text{A17})$$

where $A = \{+, \times\}$ and

$$H_A(f) := \frac{q_A}{2I} \frac{f^2}{f_0^2(1 + i\phi_{\text{rot}}) - f^2}. \quad (\text{A18})$$

Next, consider the relation between the moment of inertia I and the quadrupole moments q_+ and q_\times . If the bar shape is a rectangular cuboid with mass M and length along each axis l_x and l_y , we can write I , q_+ , and q_\times as

$$I = \int_V dV \rho (x^2 + y^2) = \frac{1}{12} M (l_x^2 + l_y^2), \quad (\text{A19})$$

$$q_+ = \int_V dV \rho (-2xy) = 0, \quad (\text{A20})$$

$$q_\times = \int_V dV \rho (x^2 - y^2) = \frac{1}{12} M (l_x^2 - l_y^2) \quad (\text{A21})$$

If the bar is along the x -axis and the aspect ratio is large enough, $l_x \gg l_y$, we can approximate $q_\times / I \simeq 1$, and we obtain

$$H_+(f) = 0, \quad H_\times(f) \simeq \frac{1}{2} \frac{f^2}{f_0^2(1 + i\phi_{\text{rot}}) - f^2}. \quad (\text{A22})$$

References

- Abbott, B.P.; Abbott, R.; Abbott, T.; Abernathy, M.R.; Acernese, F.; Ackley, K.; Adams, C.; Adams, T.; Addesso, P.; Adhikari, R.X.; et al. [LIGO Scientific Collaboration and Virgo Collaboration] Observation of Gravitational Waves from a Binary Black Hole Merger. *Phys. Rev. Lett.* **2016**, *116*, 061102. [[CrossRef](#)] [[PubMed](#)]
- LIGO Scientific Collaboration; Virgo Collaboration; KAGRA Collaboration. [LIGO Scientific Collaboration, Virgo Collaboration, and KAGRA Collaboration] GWTC-3: Compact Binary Coalescences Observed by LIGO and Virgo during the Second Part of the Third Observing Run. *Phys. Rev. X* **2023**, *13*, 041039. [[CrossRef](#)]
- Danzmann, K. et al. [LISA Study Team]. LISA: Laser interferometer space antenna for gravitational wave measurements. *Class. Quantum Gravity* **1996**, *13*, A247. [[CrossRef](#)]
- Kawamura, S.; Ando, M.; Seto, N.; Sato, S.; Nakamura, N.; Tsubono, K.; Kanda, N.; Tanaka, T.; Yokoyama, J.; Funaki, I.; et al. The Japanese space gravitational wave antenna: DECIGO. *Class. Quantum Gravity* **2011**, *28*, 094011. [[CrossRef](#)]
- Zhan, M.S.; Wang, J.; Ni, W.T.; Gao, D.F.; Wang, G.; He, L.X.; Li, R.B.; Zhou, L.; Chen, X.; Zhong, J.Q.; et al. ZAIGA: Zhaoshan long-baseline atom interferometer gravitation antenna. *Int. J. Mod. Phys. D* **2020**, *29*, 1940005. [[CrossRef](#)]
- Canuel, B.; Bertoldi, A.; Amand, L.; Pozzo di Borgo, E.; Chantrait, T.; Danquigny, C.; Dovale Álvarez, M.; Fang, B.; Freise, A.; Geiger, R.; et al. Exploring gravity with the MIGA large scale atom interferometer. *Sci. Rep.* **2018**, *8*, 14064. [[CrossRef](#)]
- Moody, M.V.; Paik, H.J.; Canavan, E.R. Three-axis superconducting gravity gradiometer for sensitive gravity experiments. *Rev. Sci. Instrum.* **2002**, *73*, 3957–3974. [[CrossRef](#)]
- Paik, H.J.; Griggs, C.E.; Moody, M.V.; Venkateswara, K.; Lee, H.M.; Nielsen, A.B.; Majorana, E.; Harms, J. Low-frequency terrestrial tensor gravitational-wave detector. *Class. Quantum Gravity* **2016**, *33*, 075003. [[CrossRef](#)]
- Ando, M.; Ishidoshiro, K.; Yamamoto, K.; Yagi, K.; Kokuyama, W.; Tsubono, K.; Takamori, A. Torsion-Bar Antenna for Low-Frequency Gravitational-Wave Observations. *Phys. Rev. Lett.* **2010**, *105*, 161101. [[CrossRef](#)]
- Braginskii, V.B.; Zel'dovich, Y.B.; Rudenko, V.N. Reception of Gravitational Radiation of Extraterrestrial Origin. *ZhETF Pisma Redaktsiiu* **1969**, *10*, 437.
- Braginsky, V.B.; Nazarenko, V.S. Heterodyne method for detecting gravitational radiation. *Mosc. Univ. Phys. Bull.* **1971**, *1*, 89.
- Matsubayashi, T.; aki Shinkai, H.; Ebisuzaki, T. Gravitational Waves from Merging Intermediate-Mass Black Holes. *Astrophys. J.* **2004**, *614*, 864. [[CrossRef](#)]
- Reisswig, C.; Ott, C.D.; Abdikamalov, E.; Haas, R.; Mösta, P.; Schnetter, E. Formation and Coalescence of Cosmological Supermassive-Black-Hole Binaries in Supermassive-Star Collapse. *Phys. Rev. Lett.* **2013**, *111*, 151101. [[CrossRef](#)] [[PubMed](#)]
- Maggiore, M. Gravitational wave experiments and early universe cosmology. *Phys. Rep.* **2000**, *331*, 283–367. [[CrossRef](#)]
- Saulson, P.R. Terrestrial gravitational noise on a gravitational wave antenna. *Phys. Rev. D* **1984**, *30*, 732–736. [[CrossRef](#)]
- Shimoda, T.; Juhel, K.; Ampuero, J.P.; Montagner, J.P.; Barsuglia, M. Early earthquake detection capabilities of different types of future-generation gravity gradiometers. *Geophys. J. Int.* **2020**, *224*, 533–542. [[CrossRef](#)]
- Punturo, M.; Abernathy, M.; Acernese, F.; Allen, B.; Andersson, N.; Arun, K.; Barone, F.; Barr, B.; Barsuglia, M.; Beker, M.; et al. The Einstein Telescope: A third-generation gravitational wave observatory. *Class. Quantum Gravity* **2010**, *27*, 194002. [[CrossRef](#)]
- Abbott, B.P.; Abbott, R.; Abbott, T.D.; Abernathy, M.R.; Ackley, K.; Adams, C.; Addesso, P.; Adhikari, R.X.; Adya, V.B.; Affeldt, C.; et al. Exploring the sensitivity of next generation gravitational wave detectors. *Class. Quantum Gravity* **2017**, *34*, 044001. [[CrossRef](#)]
- Driggers, J.C.; Harms, J.; Adhikari, R.X. Subtraction of Newtonian noise using optimized sensor arrays. *Phys. Rev. D* **2012**, *86*, 102001. [[CrossRef](#)]
- Harms, J.; Venkateswara, K. Newtonian-noise cancellation in large-scale interferometric GW detectors using seismic tiltmeters. *Class. Quantum Gravity* **2016**, *33*, 234001. [[CrossRef](#)]

21. Hughes, S.A.; Thorne, K.S. Seismic gravity-gradient noise in interferometric gravitational-wave detectors. *Phys. Rev. D* **1998**, *58*, 122002. [[CrossRef](#)]
22. Somiya, K. et al. [KAGRA Collaboration]. Detector configuration of KAGRA—the Japanese cryogenic gravitational-wave detector. *Class. Quantum Gravity* **2012**, *29*, 124007. [[CrossRef](#)]
23. Creighton, T. Tumbleweeds and airborne gravitational noise sources for LIGO. *Class. Quantum Gravity* **2008**, *25*, 125011. [[CrossRef](#)]
24. Bajpai, R.; Tomaru, T.; Suzuki, T.; Yamamoto, K.; Ushiba, T.; Honda, T. Estimation of Newtonian noise from the KAGRA cooling system. *Phys. Rev. D* **2023**, *107*, 042001. [[CrossRef](#)]
25. Chua, S.S.Y.; Holland, N.A.; Forsyth, P.W.F.; Kulur Ramamohan, A.; Zhang, Y.; Wright, J.; Shaddock, D.A.; McClelland, D.E.; Slagmolen, B.J.J. The torsion pendulum dual oscillator for low-frequency Newtonian noise detection. *Appl. Phys. Lett.* **2023**, *122*, 201102. [[CrossRef](#)]
26. Harms, J.; Ampuero, J.P.; Barsuglia, M.; Chassande-Mottin, E.; Montagner, J.P.; Somala, S.N.; Whiting, B.F. Transient gravity perturbations induced by earthquake rupture. *Geophys. J. Int.* **2015**, *201*, 1416–1425. [[CrossRef](#)]
27. Kame, N.; Kimura, M. The fundamental nature of a transient elastic response to prompt gravity perturbations. *Geophys. J. Int.* **2019**, *218*, 1136–1142. [[CrossRef](#)]
28. Kame, N. Pre-P gravity signals from dynamic earthquake rupture: Modelling and observations. *Philos. Trans. R. Soc. A Math. Phys. Eng. Sci.* **2021**, *379*, 20200136. [[CrossRef](#)]
29. Shimoda, T. Cryogenic Torsion Pendulum for Observing Low-frequency Gravity Gradient Fluctuation. Ph.D. Thesis, The University of Tokyo, Tokyo, Japan, 2020. [[CrossRef](#)]
30. Ishidoshiro, K.; Ando, M.; Takamori, A.; Takahashi, H.; Okada, K.; Matsumoto, N.; Kokuyama, W.; Kanda, N.; Aso, Y.; Tsubono, K. Upper Limit on Gravitational Wave Backgrounds at 0.2 Hz with a Torsion-Bar Antenna. *Phys. Rev. Lett.* **2011**, *106*, 161101. [[CrossRef](#)]
31. Shoda, A. Development of a High-Angular-Resolution Antenna for Low-Frequency Gravitational-Wave Observation. Ph.D. Thesis, The University of Tokyo, Tokyo, Japan, 2015. [[CrossRef](#)]
32. Shimoda, T.; Aritomi, N.; Shoda, A.; Michimura, Y.; Ando, M. Seismic cross-coupling noise in torsion pendulums. *Phys. Rev. D* **2018**, *97*, 104003. [[CrossRef](#)]
33. Ishidoshiro, K. Search for Low-Frequency Gravitational Waves Using a Superconducting Magnetically-Levitated Torsion Antenna. Ph.D. Thesis, The University of Tokyo, Tokyo, Japan, 2010.
34. Kuwahara, Y.; Shoda, A.; Eda, K.; Ando, M. Search for a stochastic gravitational wave background at 1–5 Hz with a torsion-bar antenna. *Phys. Rev. D* **2016**, *94*, 042003. [[CrossRef](#)]
35. Reid, S.; Cagnoli, G.; Crooks, D.; Hough, J.; Murray, P.; Rowan, S.; Fejer, M.; Route, R.; Zappe, S. Mechanical dissipation in silicon flexures. *Phys. Lett. A* **2006**, *351*, 205–211. [[CrossRef](#)]
36. Shimoda, T.; Ando, M. Nonlinear vibration transfer in torsion pendulums. *Class. Quantum Gravity* **2019**, *36*, 125001. [[CrossRef](#)]
37. Matichard, F.; Evans, M. Review: Tilt-Free Low-Noise Seismometry. *Bull. Seismol. Soc. Am.* **2015**, *105*, 497–510. [[CrossRef](#)]
38. Takano, S. Cryogenic Monolithic Interferometer for Low-Frequency Gravitational Wave Observation. Ph.D. Thesis, The University of Tokyo, Tokyo, Japan, 2024.
39. Shimoda, T.; Miyazaki, Y.; Enomoto, Y.; Nagano, K.; Ando, M. Coherent angular signal amplification using an optical cavity. *Appl. Opt.* **2022**, *61*, 3901–3911. [[CrossRef](#)]
40. Maggiore, M. *Gravitational Waves: Volume 1: Theory and Experiments*; Oxford University Press: Oxford, UK, 2007. [[CrossRef](#)]

Disclaimer/Publisher’s Note: The statements, opinions and data contained in all publications are solely those of the individual author(s) and contributor(s) and not of MDPI and/or the editor(s). MDPI and/or the editor(s) disclaim responsibility for any injury to people or property resulting from any ideas, methods, instructions or products referred to in the content.